Effect of CO_2 phase states and flow rate
on salt precipitation in shale caprocks – a microfluidic study

Mohammad Nooraiepour [a, *], Hossein Fazeli [a], Rohaldin Miri [a], Helge Hellevang [a, b]

[a] Department of Geosciences, University of Oslo (UiO), P.O. Box 1047 Blindern, 0316 Oslo, Norway

[b] The University Centre in Svalbard (UNIS), P.O. Box 156, 9171 Longyearbyen, Norway

[*] Corresponding author: Mohammad Nooraiepour (mohammad.nooraiepour@geo.uio.no)

15 Pages, 6 Figures, 1 Table

Table of Contents

List of Figures

List of Tables

Fabricating shale samples

To prepare shale specimens for fabrication of microfluidic specimens and laser-scribing, we cut the organic-rich shales of Draupne Formation in less than 2.5 cm diameter sizes to fit the plastic molds in Figure S1. Figure S1 shows the plastic mold that we used to fabricate the specimens in addition to the final prepared sample. The shale samples were dried at 40°C for three days to reduce the initial brine saturation within the matrix and make them ready for putting inside the epoxy resin. We decided to fabricate the specimens using the cold mounting procedure to minimize potential alterations of the shale substrate. In the cold mounting procedure, the dried samples were placed inside a cylindrical plastic mold with 2.5 cm and 1.5 cm diameter and height, respectively, where the epoxy resin was added to the mold to fill it completely (Fig. S1b and e). Given the pore space characteristics of the Draupne shale, the epoxy cannot enter the pore volume within the matrix. However, the friable, brittle, and porous materials can be vacuumed before adding the epoxy, or the sample can be impregnated with epoxy under vacuum if it is necessary. The mold (shale sample surrounded by epoxy) was then left overnight to harden. Then, we took the mold's cap out (Fig. S1a and d) to retrieve the hardened specimen. Subsequently, a series of automatic grinding and polishing steps were followed to (a) reach the surface of shale substrate and remove the overlying epoxy, and (b) provide a flat unscratched surface for laser scribing of designed fracture patterns. The final shale specimen before scribing the laser patterns is shown in Figure S1c and f. As is illustrated in top and side views, the shale material is surrounded by dried epoxy resin (Fig. S1). The cold mounting procedure does not change properties of the shale material. The injected fluids (bine and CO_2 phases) were partly in contact with epoxy at the inlet and outlet. However, no interaction between the epoxy and injectant is expected, and the epoxy plays a role as a non-reactive material within the system.
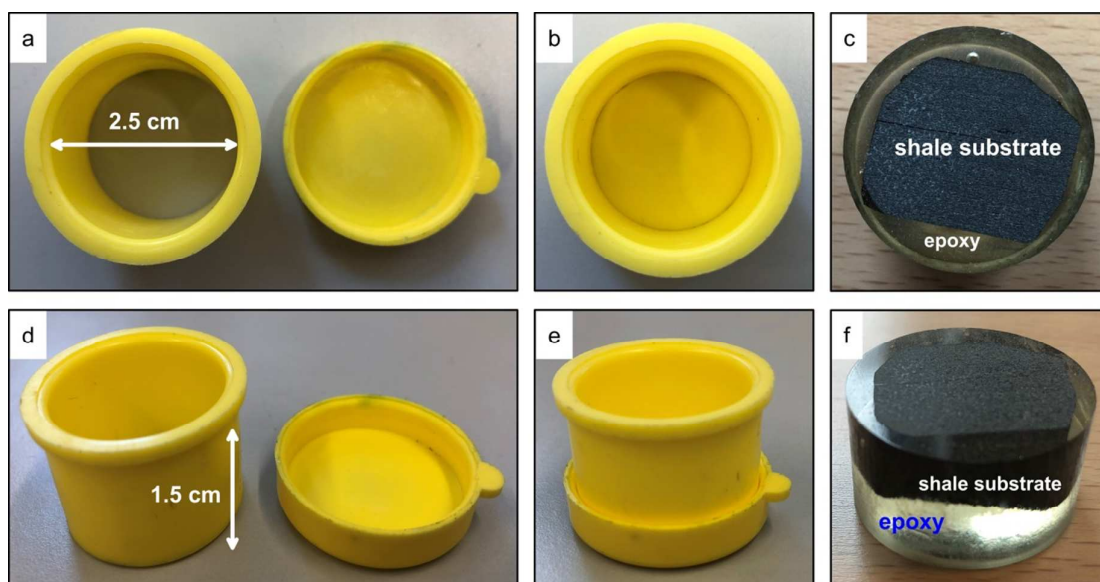
Figure S1. Fabrication of microfluidic specimen. (top) top view (bottom) side view of plastic mold (a-e) and microfluidic shale sample (c and f)

Preparing microfluidic specimen and mounting it into the pressure vessel

When we completed fabrication of shale specimens (Fig. S1), we laser-scribed the fracture network on the surface of the shale substrate. To scribe the designed fracture pattern on the shale specimens, we used a Rofin scribing laser at the microsystems and nanotechnology laboratory (MiNaLab) at the University of Oslo (UiO). It is an air-cooled solid-state laser cutter with the continuous-wave operation and Q-switch assembly that provides high performance and precision pulses. A CombiLine workstation houses the PowerLine E Air 25 laser maker and provides integrated computer control and programmable z-axis positioning of the marking head. The CombiLine system (Rofin) is equipped with visual laser marker software, which allows direct transmission of required marking data from computer to the laser marker. The fracture network was scribed using a 532 nm scribing laser at 25A, 15000 Hz and 200 mm/s. The scribing was performed twice with an interval time of 5 minutes between each execution to keep the sample heating to a minimum. Moreover, a high scanning speed, high power, and low frequency were selected to maximize ablation, minimize heating of the sample, and limit the heat affected zone. The laser-scribed fracture network is 19 mm long and 14 mm wide pattern. Subsequently, the ablated debris and heat affected material were cleaned to reach the undisturbed matrix of the shale specimen inside the fracture network. To remove the ablated debris, we used micro-scratcher blades under an optical microscope. The scratching procedure and micro-scale cleaning did not change the geometry of scribed patterns, but only widened and deepened the fracture branches. Surface profilometry was then performed to capture geometry and dimensions of the eventual fracture planes before the experiment.

Figure S2 demonstrates a SEM micrograph of a part of fracture pattern, where two channels cross each other. A closer picture of the laser-scribed pattern is presented in Figure S2b, where the ablated geomaterial still lies within the fracture plane. The fracture planes after removing the heat-affected remains and cleaning the surfaces are shown in Figure 2Sc. The EDS analyses indicated a close similarity in elemental composition and a resemblance in the microstructure of the laser-scribed regions and neighboring areas. Figure S2d demonstrates an exemplary plot of surface profilometry on the shale micromodel. A straight part of the channel is analyzed, which shows an average width and depth of 500 ± 100 μm and 400 ± 25 μm, respectively (Fig. S2d).

After cleaning the heat-affected debris, the microfluidic shale specimen was ready to be mounted in the experimental pressure vessel. A close-up SEM micrograph of cleaned fracture planes is given in Figure S3. As shown in Figure 2a, there is sample holder in the bottom pedestal to house the microfluidic specimen. The height of microfluidic specimen is designed to be a bit higher (approximately 500-1000 μm) than the depth of the sample holder. While the bottom pedestal provides hydraulic connection to the fluid inlet and outlet and holds the specimen, the top cap carries the monitoring window and seals the pressure vessel. In addition to the top cap, an O-ring outside the perimeter of the specimen in the bottom pedestal keeps the injectant inside the pressurized chamber of

the cell. In this way, the pressure vessel is completely sealed even at high pressures. Adjusting the proper height of the sample ensured that we have a good contact between the top of the shale specimen and viewing glass to prevent communications between the channels. Another consideration to ensure complete sealing of the microfluidic specimen was incorporating six screws in the pressure vessel (60º interval). The long screws connected the top and bottom caps. They are also tightened enough to completely press the glass window on the top of the shale specimen and the surrounding O-ring. Through such a design, we assured active stress between the sealing surface and the shale specimen. Since the top section of the shale specimen was under stress, so the scribed fracture patterns were sealed and separated from each other. However, because of the ductile nature of organic-rich shales of Draupne Formation, local deformations might be formed that produced a transition between the channel and complete sealing at the top of the shale specimen. Such deformations, in particular, may be found near the fracture walls where they were in contact with the sealing glass window.
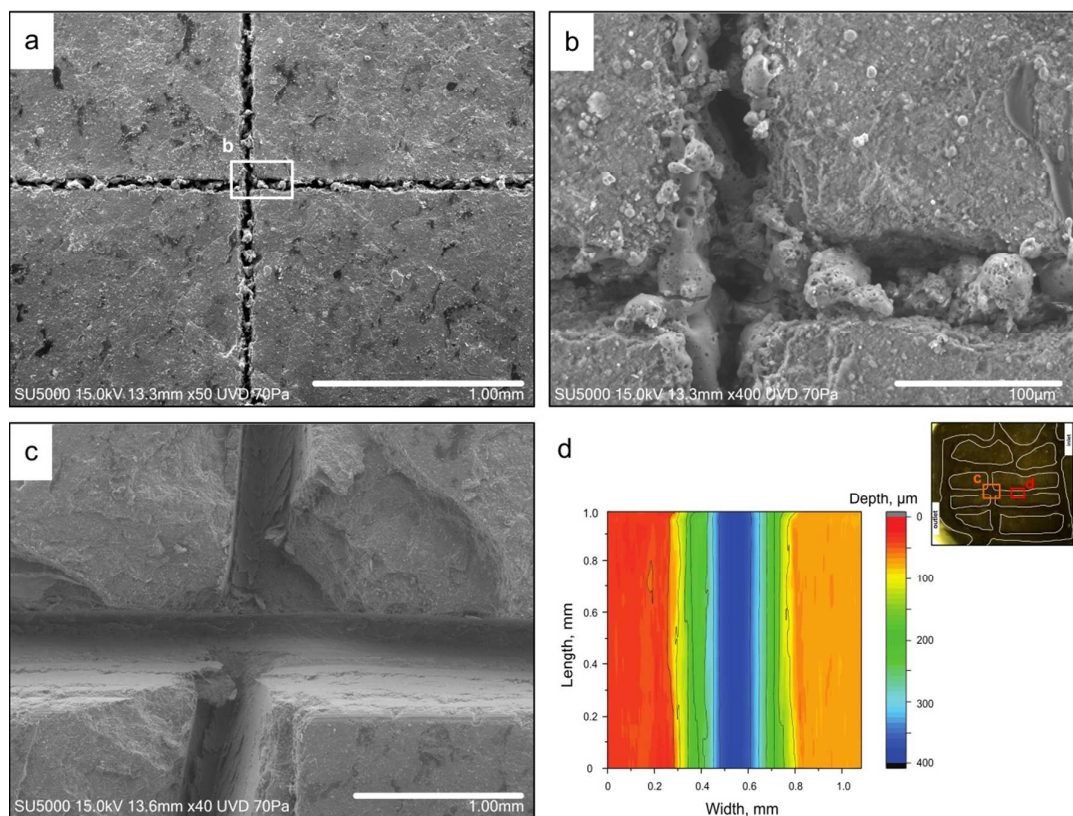
Figure S2. (a) SEM micrograph of fracture pattern on the surface of the shale specimen, boxed region expanded in (b) The laser-scribed pattern, where the ablated geomaterial still present within the fractures; (c) The SEM micrograph of cleaned fracture plane after removing the heat-affected remains; (d) The results of surface profilometry after cleaning fracture planes from the heat-affected remains.
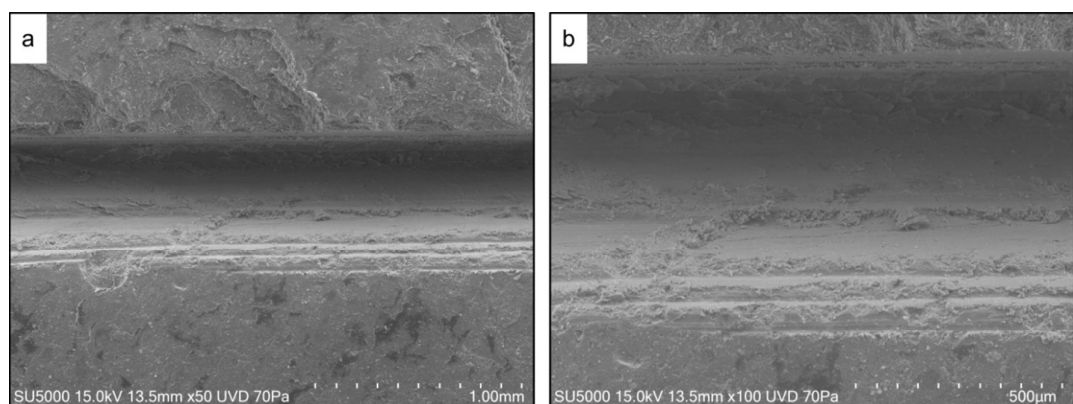
Figure S3. A close-up SEM micrograph of the laser-scribed pattern, where the ablated geomaterial are cleaned from the fracture plane

Experimental conditions

In this study, we conducted microfluidic experiments to investigate the effect of CO_2 phase states on salt precipitation at nine pressure-temperature conditions, combining temperature of 22, 40 and 60°C, with three pressures (1, 5 and 8 MPa). The experiments were performed at a flow rate of 20 cm^3 CO_2/min. In addition, to study the impact of CO_2 injection flow rate on the distribution and extent of salt precipitation, we injected gaseous (1 MPa) and supercritical CO_2 (8 MPa) with three different flow rates (5, 10 and 20 cm^3 CO_2/min) at 60°C. A summary of performed experiments is given in Table S1.

Table S1. Summary of the performed experiments in this study

	injection flow rate (cm^3 CO_2/min)	Pressure (MPa)	Temperature (°C)	CO_2 phase state
Effect of CO_2 phase states (pressure-temperature conditions)	20	1	22	gas
	20	5	22	gas
	20	8	22	liquid
	20	1	40	gas
	20	5	40	gas
	20	8	40	super-critical
	20	1	60	gas
	20	5	60	gas
	20	8	60	super-critical
Effect of injection flow rate	20	1	60	gas
	10	1	60	gas
	5	1	60	gas
	20	8	60	super-critical
	10	8	60	super-critical
	5	8	60	super-critical

Analyzing surface coverage of salt crystals

To analyze surface coverage of precipitated salt crystals, the obtained experimental images were extracted from the recorded videos (1-hour intervals) and processed following the published workflows.[50, 58-60] First, several filters were applied to improve tone, enhance contrast and reduce noises. The optical 2D images were then segmented into shale and salt components to quantify surface coverage of the salt crystals. The salt surface coverage considers only the salt accumulations inside the fracture network, and presents the results as the percentage of the total surfaces occupied by the fracture branches. To refine the boundaries and help differentiate between dried shale matrix and precipitated salts, manual modifications were also performed. The manual corrections were also necessary because the color of the shale matrix changed over time and became brighter. The color change from dark to light grey during the experiments happened because CO_2 gradually dried residual brine inside the fractures in addition to the saturation of shale matrix.

Flow mechanisms

Three flow mechanisms influenced saturation of brine within the microfluidic specimen. Initially, the microfluidic sample (fracture network and shale matrix) was completely saturated with the prepared brine. Figure S4 shows how different flow mechanism changed the saturation of brine within the microfluidic specimen and dried the sample through injection of CO_2 phases for the P8T60Q10 experiment. The notations stand for P= pressure, T= temperature, Q= flow rate. As is shown in Figure S4.a, the saturated shale sample looks homogenous with dark grey color. When we opened the inlet valve, pressurized CO_2 pushed the brine outside the fracture network through two-phase viscous displacement regime. As a result, various forms of saturation patches (pools, domes and water films on fracture surfaces) were formed in the fracture pore volume due to capillary forces (Fig S4b). The experimental elapsed time during which viscous displacement was dominating is relatively short. It continued less than 10 minutes, while the whole experiment lasted for 16 hours. Finally, an evaporation regime prevailed. The evaporation regime dried the residual brine saturation inside the fracture network and matrix of the shale micromodel. The color of the shale specimen, therefore, gradually changed from the dark grey in Figure S4b to light grey in in Figure S4c. As evaporation continued and salt concentration in the remaining brine inside the fracture network reached the solubility limit, precipitation of micrometer-sized halite crystals started near the inlet (Fig S4c). Figure S5 illustrates that adjacent and detached salt bodies have an affinity for growth toward each other. It also demonstrates that micrometer-sized halite crystals on the fracture surfaces grew very fast once precipitation started, and separate patches became connected. Despite massive precipitation pattern of the micrometer-sized salts, closer observation revealed that these aggregates have a porous structure of densely precipitated crystals. Figure S6 presents a series of experimental images that are recorded at the end of the different experiment, and they show microstructure of precipitated micrometer-sized halite crystals on the fracture walls.
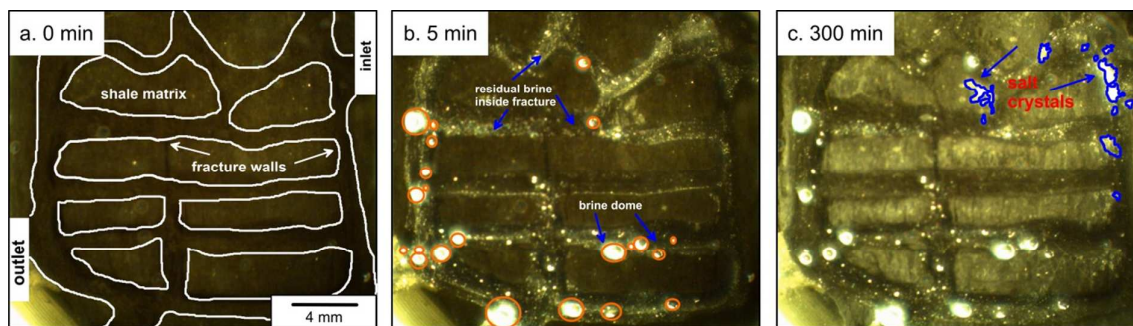
Figure S4. Effect of different flow mechanism on changing the saturation of brine within the microfluidic specimen. (a) fully brine-saturated fracture network and shale matrix before the start of the CO_2 injection. (b) residual saturation inside the fracture network after two-phase viscous displacement and due to capillary forces. (c) An experimental image during evaporation regime, during which residual brine saturation was drying, and salt crystals were precipitating. The subfigures are time-lapse images of an experiment at pressure = 8 MPa, temperature = 60°C, and flow rate = 10 cm^3 CO_2/min. The white-outlined surfaces describe the fracture walls, and the blue-outlined areas inside the fractures are precipitated salt crystals.

Figure S5. The growth and distribution pattern of micrometer-sized salt crystals salt precipitation on the interface of rock and CO_2 stream. It shows the affinity of neighboring salt bodies for growth toward each other and become connected. The subfigures are time-lapse images of an experiment at pressure = 1 MPa, temperature = 60°C, and flow rate = 10 cm^3 CO_2/min. The white-outlined surfaces describe the fracture walls, and the blue-outlined areas inside the fractures are precipitated salt crystals.
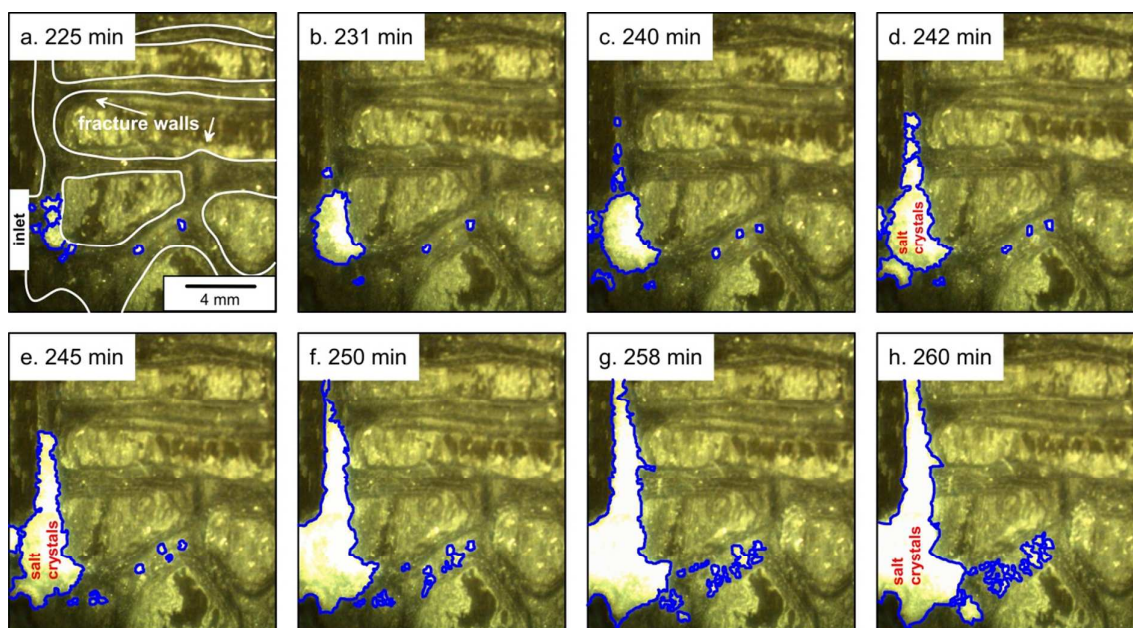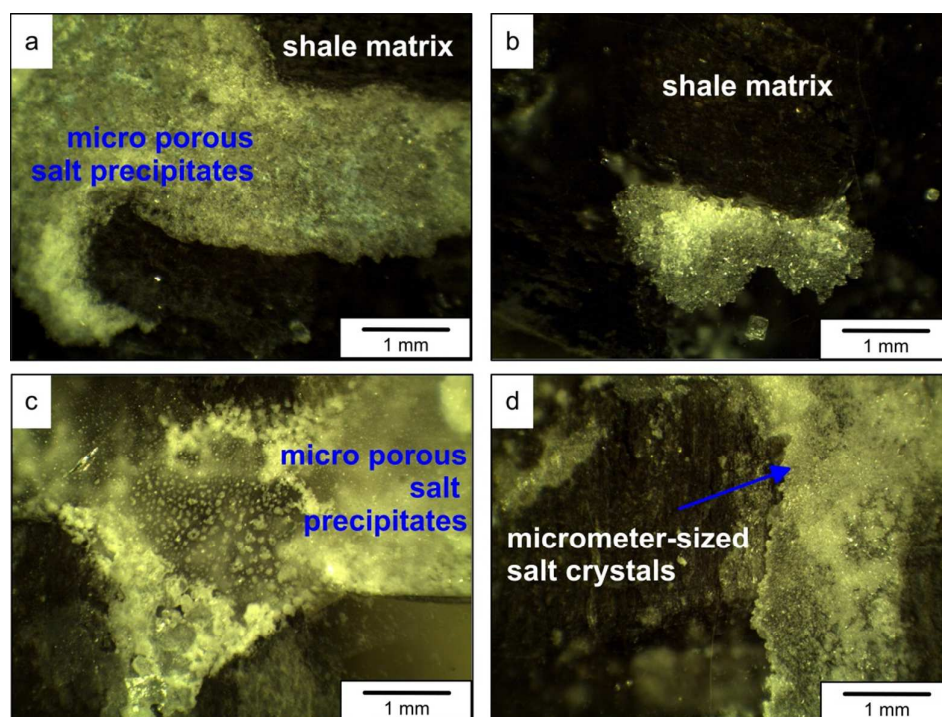
Figure S6. A series of experimental images that illustrate microstructure of micrometer-sized halite crystals. The salt crystals are precipitated on the fracture walls, and usually are less than 20 μm in size. The images are taken at the end of the experiment in different pressure-temperature conditions. The precipitated salt bodies produce a low-porosity low-permeability medium with potentially large capillarity.

Description of experimental videos

In addition to the present document as the Supporting Information, we have provided the reader with two videos from the microfluidic salt experiments:

- Video 1. The dynamics of growth for a large single cubic crystal of halite in the aqueous phase. The experiment was performed at pressure = 5 MPa, temperature = 22°C, and flow rate = 20 cm^3 CO_2/min.

- Video 2. The dynamics of salt precipitation for micrometer-sized crystals of halite that form on the interface of rock and CO_2 stream. The experiment was performed at pressure = 1 MPa, temperature = 22°C, and flow rate = 20 cm3 CO2/min.

The pulses of fluid movement that may be visible in the above videos are artifacts due to the fast-forwarding the videos, which is 500-1000 times faster than the experimental time. The pulses might also be present due to slight pressure variation when one pump switched to another pump during the refill. We used a dual-cylinder syringe pump (Teledyne Isco, 100DM), which controlled CO_2 flow rates.